RSC Advances

ROYAL SOCIETY OF CHEMISTRY

www.rsc.org/advances

Synthesis of Curved Si Flakes Using Mg Powder as Both Template and Reductant and Their Derivatives for Lithium-Ion Batteries

*Jian Zhu, Da Deng**

Department of Chemical Engineering and Materials Science, Wayne State University,

5050 Anthony Wayne Dr, Detroit, Michigan, United States, 48202

Keywords: silicon flakes, magnesiothermic reduction, active template, lithium ion batteries.

TOC

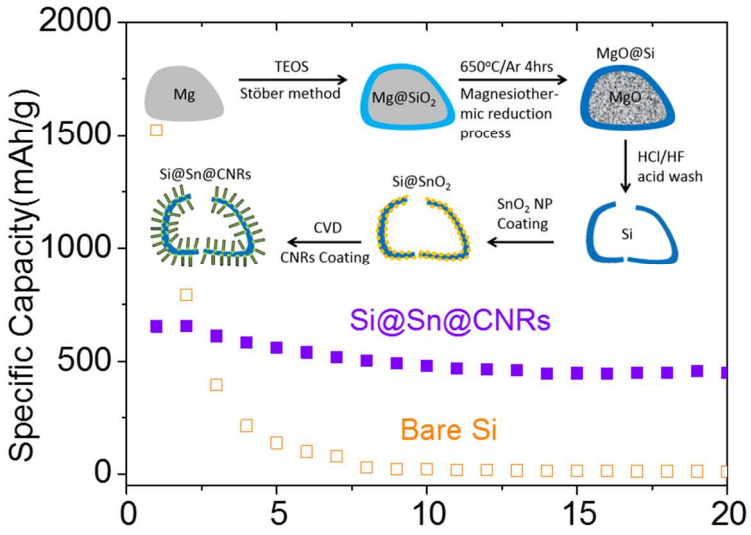

ABSTRACT

Silicon has been considered as one of the most promising carbon-alternative anode materials for high-energy lithium-ion batteries (LIBs). However, it is still challenging to facilely prepare Si with unique micro-/nano- structures on a large scale. Here, we report a designed procedure for the synthesis of curved Si microflakes. Commercial Mg powder was used as both the active template for SiO_2 coating and reductant to subsequently reduce SiO_2 sheaths into Si by magnesiothermic reaction, for the first time. The as-obtained curved Si flakes could be further tailored. We demonstrated that Sn@Carbon nanorods (CRNs) could be formed on the surface of curved Si flakes forming Si@Sn@CNR composite. When tested as anode materials for LIBs, the as-prepared Si@Sn@CNR composites exhibited highly improved electrochemical performance as compared to pure Si materials.

1. INTRODUCTION

Lithium-ion batteries (LIBs) have been attracting much attention for decades. LIBs are considered the powerhouse of the popular mobile personal electronic devices, including cell phones and laptop computers.[1-3] LIBs are playing increasingly important roles in hybrid and electric vehicles.[4-6] To accommodate the growing demand for energy storage, tremendous efforts have been made to develop next-generation LIBs with improved electrochemical performances in terms of energy, power, cost and safety. The electrochemical performances of LIBs are determined by electrode materials selected. Regarding the anode, carbonaceous materials are still dominantly used in commercial LIBs currently. However, graphite has a low theoretical capacity of 372 mAh/g (by intercalation forming LiC_6). Therefore, next-generation LIBs should employ carbon-alternative negative electrode materials.

Among many potential carbon alternatives investigated, silicon is one of the most outstanding candidates. Silicon has the highest theoretical capacity of ~3572 mAh/g by forming $Li_{4.4}Si$ based on alloying mechanism.[4, 7-9] However, the insertion and extraction of lithium in and out silicon could lead to a very large volume variation (>300%), which cause cracking of materials and disintegration of the electrodes leading to capacity fading or poor cycling performance. To address the issue of volume variation, extensive efforts have been made to prepare nanoscale silicon. Various nanoscale silicon materials have been reported achieving certain level of success.[10, 11] For example, 1-dimentional Si nanowires were grown on stainless steel substrate by vapor–liquid–solid growth method;[9] 2-D Si nanofilms with thickness around 250 nm on Cu substrate prepared by magnetron sputtering were synthesized;[12] 3-D lotus-root-like Si was prepared through template assisted magnesiothermic reduction method.[13] Silicon materials with unique morphologies have been prepared through various methods.[12] Si has been deposited on carbon nanowire through chemical vapor deposition method using SiH_4 to prepare carbon@silicon nanowire in argon at 500^{o}C.[14] Template-assisted magnesiothermic reduction has also been applied to obtain Si from SiO_2. SBA-15 silica was used as silicon source and template to prepare 3-D mesoporous silicon.[13] TiO_2 nanorods have been used as the template coated with SiO_2 and core-shell Ti@Si coaxial nanorods have been prepared by magnesiothermic reduction process.[15] Graphene oxides have been applied as the substrate to grow SiO_2 particles, and 3-D porous structure of silicon/graphene has been prepared by magnesiothermic reduction process.[16] However, it is still very challenging to achieve facile synthesis of Si materials in micro- or nano-scale at low cost by simple procedures.

Magnesiothermic reduction of SiO_2 to silicon is a promising method to effectively produce silicon with unique micro- or nano-structures.[5, 13, 16-19] For example, magnesiothermic reduction

of micro-assemblies silica to obtain microporous nanocrystalline silicon replicas has been reported.[17] 3-D porous Si was prepared through the magnesiothermic reduction of SiO_2 mesoporous powder.[19] SiO_2 with unique structures as precursors normally have to be prepared by multi-step procedures, typically by template methods using metal, metal oxides or carbon based materials as sacrificed templates.[20] However, templates used for the preparation of silica precursors must be removed to get the silica precursors and the template removing process is typically destructive toward the products. We called those sacrificed templates as passive templates. Additional issue is that the sacrificed templates are difficult to be prepared. The complicated procedure with multiple steps and the use of expensive sacrificed templates make it challenging to mass produce silicon with unique structures. Therefore, it will be interesting to use active templates which can function as reductants at the same time.

Here, we developed a facile synthesis strategy where commercial magnesium powder was employed as multifunctional template for the coating of silica sheaths on it and also the reducing agent for magnesiothermic reduction of silica into curved silicon microflakes. We called the Mg templates as active templates. Other passive templates were not required. In other words, our synthesis strategy eliminated the complex template preparation and passive template-removing processes. Additionally, we also tried to improve the conductivity of the as-prepared silicon microflakes. Hierarchical structure of Si@Sn@CNRs to further improve the electrochemical performances of silicon microflakes was demonstrated. The preliminary results show that the electrochemical performance of Si@Sn@CNRs, which has a reversible capacity of 451 mAh/g after 20 cycles, was greatly improved as compared to pristine Si microflakes, whose capacity dropped to 10 mAh/g at the same testing condition. Figure 1 shows the schematic of the design and procedure in the preparation of curved Si microflakes and Si@Sn@CNR composites.

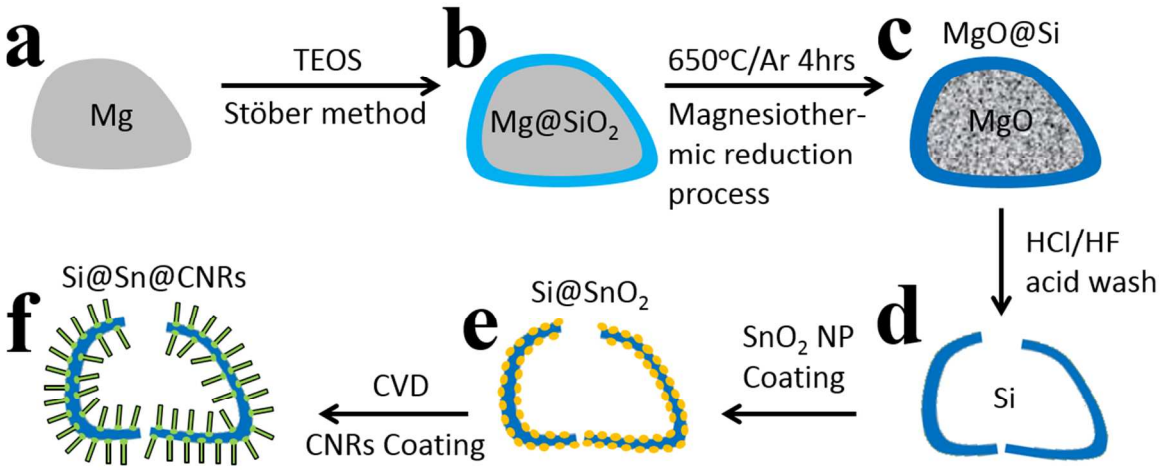

Figure 1. Schematic of the design and procedure in the preparation of curved Si flakes by using Mg powder as bifunctional template and reductant: (a) commercial Mg powder, (b) SiO_2 wrapped Mg template, (c) Si wrapped MgO obtained by magnesiothermic reduction of SiO_2 using Mg as the reductant, (d) curved Si flakes obtained by etching off MgO. Additional process to further tailor the curved Si flakes (e) SnO_2 nanoparticles decorated Si flake and (f) Si@Sn@CNRs high-order structures obtained by CVD treatment of (e).

2. EXPERIMENTAL SECTION

All the reagents used were as received. The overall idea and experimental procedure are illustrated in Figure 1.

Preparation of Mg@SiO_2: In a typical synthesis, 0.4 g of Mg powder (325 mesh) was added into 60 ml of 2-propanol under stirring, followed by 0.8 g of hexadecyltrimethyl-ammonium bromide (CTAB) and the mixture was stirred for 6 h. Then the Mg powder capped by CTAB were collected and re-dispersed into the mixture of 75 ml of 2-propanol, 16 ml of DI water and 4 ml of ammonia under stirring to form solution A. After 5 min of stirring, the mixture of 1 ml of tetraethyl orthosilicate (TEOS) and 45 ml of 2-propanol was added into solution A drop-wisely to form solution B. Solution B was kept under stirring for 12 hours. The precipitates were

washed with water and ethanol, and then dried in a vacuum oven at room temperature for 24 h to obtain SiO_2 wrapped Mg microparticles or Mg@SiO_2. An excessive amount of Mg was purposely used here taking into consideration of possible certain fraction of Mg oxidized in the process to ensure enough Mg for reduction of SiO_2.

Preparation of Si microflakes: Mg@SiO_2 powder was put into a tube furnace, heated to 650 ^oC with ramping rate of 10 ^oC/min in argon, and kept at 650 ^oC for another 4 hours for magnesiothermic reduction to get MgO@Si. The MgO@Si powder was washed by 2M HCl solution and then HF acid solution (5 wt%) to remove MgO and SiO_2 remnant to obtain Si phase. The acid washed sample was then washed with water until the pH value was equal to the pH value of DI-water, and then washed with ethanol. The solid sample was dried at 80^oC in a vacuum overnight.

Preparation of pure Si@Sn@CNRs: Calculated amount of silicon microflakes (0.2384 g of Si(solid), 8.5 mmol) were put into 30 ml freshly prepared aqueous solution of $SnCl_4$ (0.1 ml of $SnCl_4$ (liquid), 0.85 mmol). The mixture was stirred for 24 h to allow the $SnCl_4$ to be hydrolyzed forming SnO_2 nanoparticles deposited on the Si microflakes. The Si microflakes decorated with SnO_2 were collected by centrifugation and dried at 80^oC in a vacuum oven. To grow CNRs on Si structures, the dried silicon microflakes decorated with SnO_2 nanoparticles were put into a crucible and inserted into a tube furnace. Argon was used to purge the tube furnace for 30 min to remove the air inside the tube furnace. Tube furnace was heated to 650 ^oC with ramping rate of 10 ^oC/min under argon. The gas was switched to acetylene balanced with argon (10% of acetylene in the mixture) at rate of 100 sccm and maintained at 650 ^oC for 3 h for chemical vapor deposition (CVD) reactions. The furnace was then switched back to pure Argon flow and cooled down in Argon.

Materials Characterization: X-ray diffraction (XRD) was carried out with Rigaku Smartlab X-ray diffractometer using Cu K_α radiation (λ=0.15418 nm). The morphologies were characterized by scanning electron microscopy (JSM - 6510LV SEM, equipped with X-ray energy-dispersive spectrometer (EDS), field emission scanning electron microscopy (JSM-7600 FESEM), and transmission electron microscopy (JEOL 2010 TEM, with accelerating voltage of 200 kV).

Electrochemical Measurements: Typically, Si microflakes were mixed with conductivity enhancer (Super P carbon black, Timcal), polyvinylidene fluoride (PVDF) binder at 8:1:1 weight ratio in N-methylpyrrolidone (NMP) to form a homogenous slurry. The slurry of Si@Sn@CNRs microflakes was prepared similarly by mixing 90wt% of the as prepared active materials and 10wt% of polyvinylidene fluoride binder in N-methylpyrrolidone. Note that no conductivity enhancer of Super P carbon black was added. The slurry was then applied to copper discs as current collectors and dried in a vacuum oven at 100 ^oC for 24 h. Typically, the mass loading on the current collector for Si@Sn@CNRs is 8 mg per cm^2. CR2032-type coin cells were assembled in an argon-filled glove box using the coated copper disc as the working electrode, metallic lithium foil as the counter and reference electrodes, 1 M solution of $LiPF_6$ in a 50:50 v/v mixture of ethylene carbonate (EC) and diethyl carbonate (DEC) as the electrolyte, and PP/PE/PP trilayer membranes (Celgard 2320) as the separator. The coin cells were galvanostatically charged and discharged in the voltage window of 0.01V-2.5V on a MTI BST8-WA battery tester at room temperature.

3. RESULTS and DISCUSSION

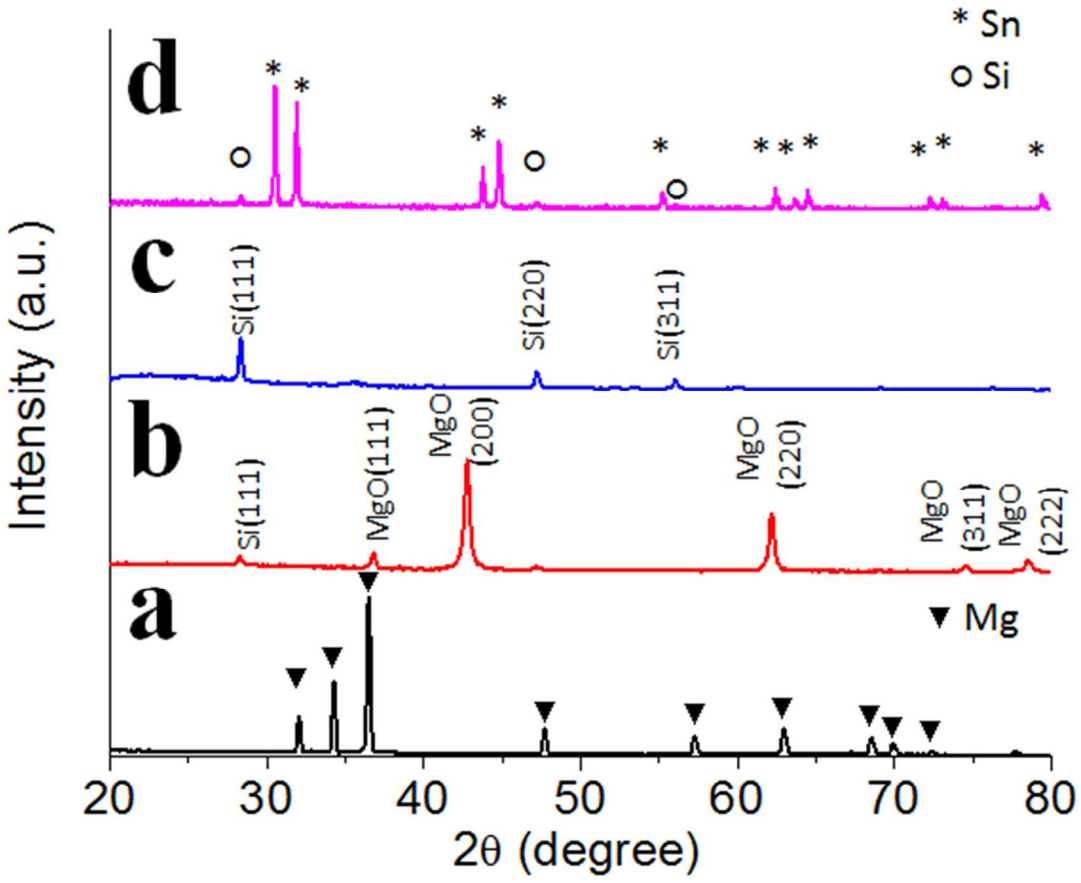

Figure 2. XRD patterns of (a) silica wrapped magnesium powder ($Mg@SiO_2$), (b) silicon wrapped magnesium oxide (MgO@Si), (c) silicon microflakes, and (d) silicon microflakes decorated with tin and carbon nanorods (Si@ Sn@ CNRs).

The chemical changes and compositions of the intermediate samples outlined in Figure 1 were characterized by XRD (Figure 2). First, a layer of SiO_2 was coated on Mg template via the Stöber sol–gel process to obtain $Mg@SiO_2$ as the precursor. Tetraethyl orthosilicate (TEOS) in our experiment was hydrolyzed and SiO_2 formed in the presence of ammonia and water (Figure 1b). This Stöber sol–gel process is popularly used for SiO_2 coating, such as SiO_2 coated metals (Au, Ag, Fe, Ni and so forth),[21] SiO_2 coated metal oxides (iron oxide[22], cobalt oxide[23], zinc oxide[24] and titanium oxide [25]) and SiO_2 coated carbon.[20, 26, 27] To the best of our knowledge, this was the first time to coat SiO_2 on Mg microparticles as the active template. Figure 2a shows the

XRD pattern of silica wrapped magnesium powder ($Mg@SiO_2$). Only XRD peaks associated with metallic magnesium are observed (JCPDS Card No.35-0821). No peaks associated with SiO_2 sheaths suggest the SiO_2 sheath is amorphous. SiO_2 sheath was subsequently reduced to Si through the magnesiothermic reduction process utilizing the Mg core as the reducing agent. Figure 2b shows the XRD pattern of MgO@Si. All the peaks can be assigned to silicon (JCPDS Card No.27-1402) and MgO (JCPDS Card No.45-0946), indicating the successful reduction of amorphous SiO_2 into Si and the oxidization of Mg core to MgO. The MgO core could be easily etched off by dilute HCl. Additionally, dilute HF was used to etch off a trace amount of remnant of SiO_2 that might not fully reduced by magnesiothermic reduction. Figure 2c shows the Si flakes after acid etching to remove MgO. All the peaks can be assigned to silicon (JCPDS Card No.27-1402) and no peak for MgO is observed (Figure 2c), indicating MgO was completely removed by etching. The Si flakes were further processed. First, SnO_2 nanoparticles were decorated on Si flakes through the hydrolysis of $SnCl_4$ in water to obtain Si@ SnO_2 nanoparticles. Subsequently, the SnO_2 deposited on the Si flakes acted as catalysts for growth of CNRs via CVD. At the same time, the SnO_2 was reduced to metallic Sn under this CVD condition and Si@Sn@CNRs was obtained. The XRD pattern of the as-prepared flakes of Si@Sn@CNRs is shown in Figure 2d. The peaks for Si can still be observed, and the all other peaks can be assigned to metallic tin (JCPDS Card No. 86-2264). This indicates that the deposited SnO_2 were completely reduced to Sn during the CVD process.

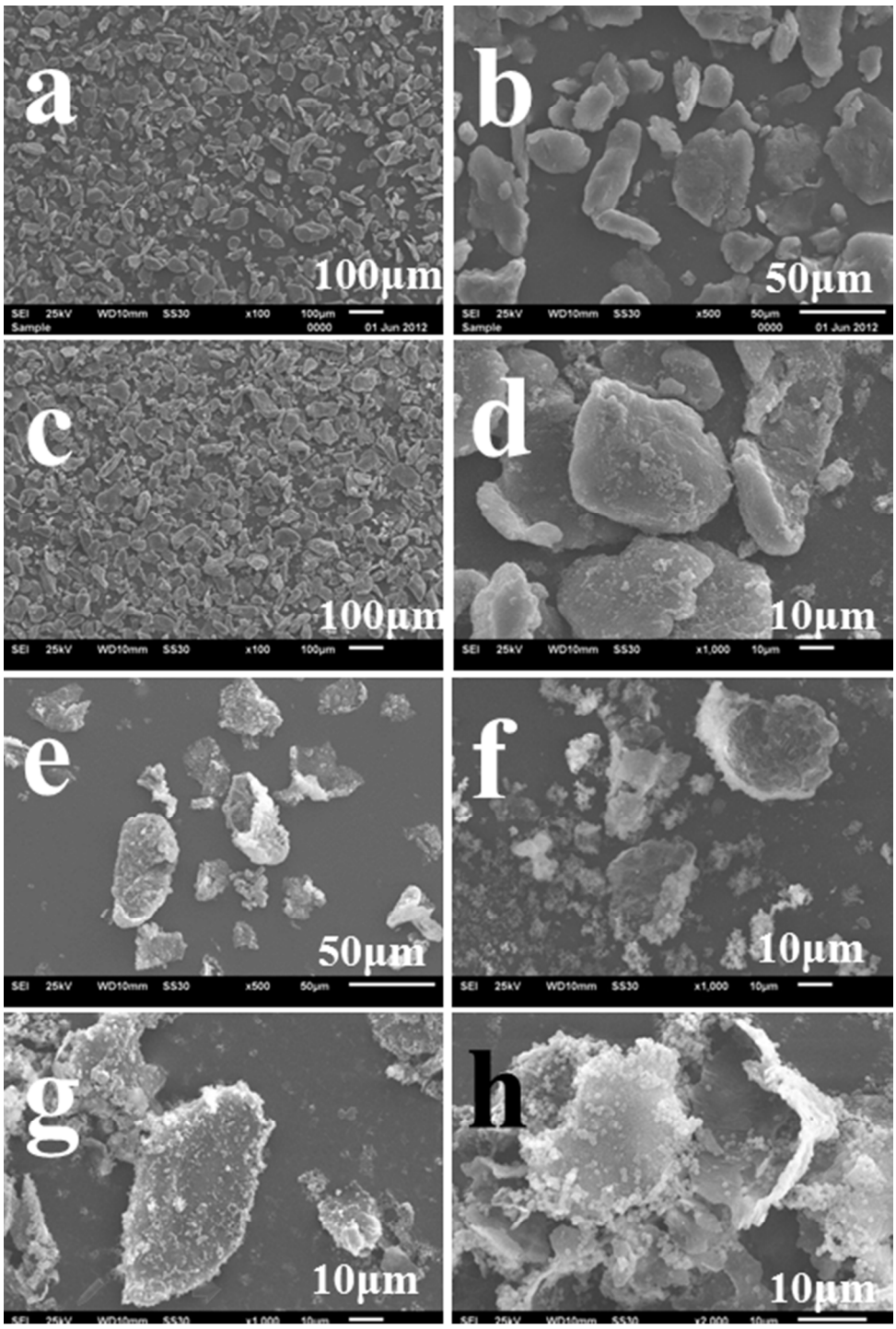

Figure 3. Scanning electron microscope (SEM) images at different magnification of (a, b) commercial Mg powder, (c, d) SiO_2 wrapped Mg powder, (e, f) Si wrapped MgO after magnesiothermic reduction process, and (g, h) curved Si flakes after acid etching.

The morphologies of products obtained at different stage of process (Figure 1. a-d) were characterized by electron microscopes (Figure 3). Figure 3a-b shows the SEM image of commercial Mg powder at different magnification. The size of Mg powder is about 40 to 90 μm. The Mg powder is in the form of plates or bulk rods. The low and high magnification SEM images of SiO_2 wrapped Mg are shown in Figure 3c and Figure 3d, respectively. The overall size and morphology of the Mg@SiO_2 are almost the same as the Mg powder without SiO_2 wrapping. Figure 3e, the low magnification SEM image shows the morphology of the MgO@Si obtained after the magnesiothermic reduction process. Compared to the Mg template or Mg@SiO_2, the size of the structure of the MgO@Si is reduced. The Mg was converted to MgO during the reaction and the volume of the core would change due to the different density of Mg (1.74 g/cm^3 at room temperature) and MgO (3.58 g/cm^3). Therefore, the Si shells could collapse into small pieces due to shrinking core. On the other hand, Mg template (also the reductant) may be melted due to its low melting point of 650^oC, left over the Si shells. The magnesiothermic reaction in reduction of SiO_2 into Si could involve both liquid and vapor phase Mg.[28] Figure 3f shows the high magnification SEM image of the MgO@Si, where curved flake-like structure in micro scale can be observed. The Si microflakes obtained after acid etching to remove MgO and trace SiO_2 are shown in Figure 3g and Figure 3h. Curved Si flakes are observed reflecting the heritage of template used (figure 3h). These results evidenced that Mg powder play dual roles as both template and reductant in the formation of Si microflakes. We believe the same idea could be extended to achieve unique structured Si sheaths using Mg in other unique structures (e.g., Mg nanospheres, nanoplates, nanorods, nanourchins, etc.[29, 30]) as the active template and reductant to form desired Si structures.

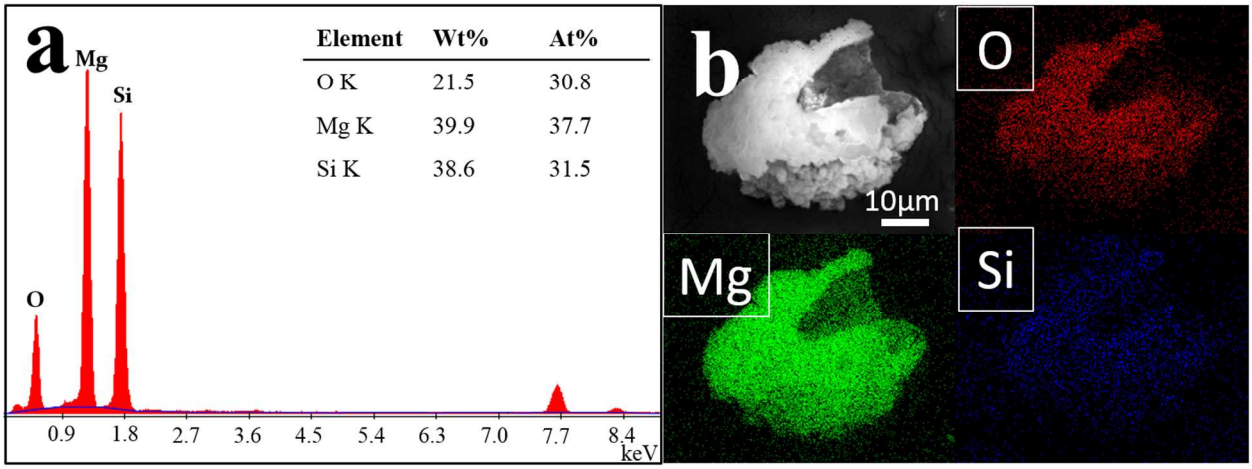

Figure 4. (a) EDS, (b) SEM image and corresponding elemental mapping of MgO@Si to show the even distribution of O(Red), Mg (Green) and Si(Blue).

To confirm the bifuntional roles played by the Mg powder as template and reductant, EDS analysis and elemental mapping were carried out for the intermediate compound of MgO@Si (Figure 4). The composition of the MgO@Si after the magnesiothermic reduction process was Mg, O and Si, as revealed by EDS (Figure 4a). The elements could be associated with the presence of MgO, Si and a trace amount of amorphous SiO_2, A section of Si sheath with MgO was further analyzed by elemental mapping (Figure 4b). The mouth-like opening suggests the Mg core as template was melt and the Si sheath wrapping the core was broken after magnesiothermic reaction. The corresponding elemental mapping of the MgO@Si flake clearly shows the uniform element distribution of O (red), Mg (green) and Si (blue) in the structure. The broken of the freshly formed Si sheath could also be attributed to the MgO nanoparticles formed inside the Si sheath and MgO nanoparticles induced low mechanical stability.

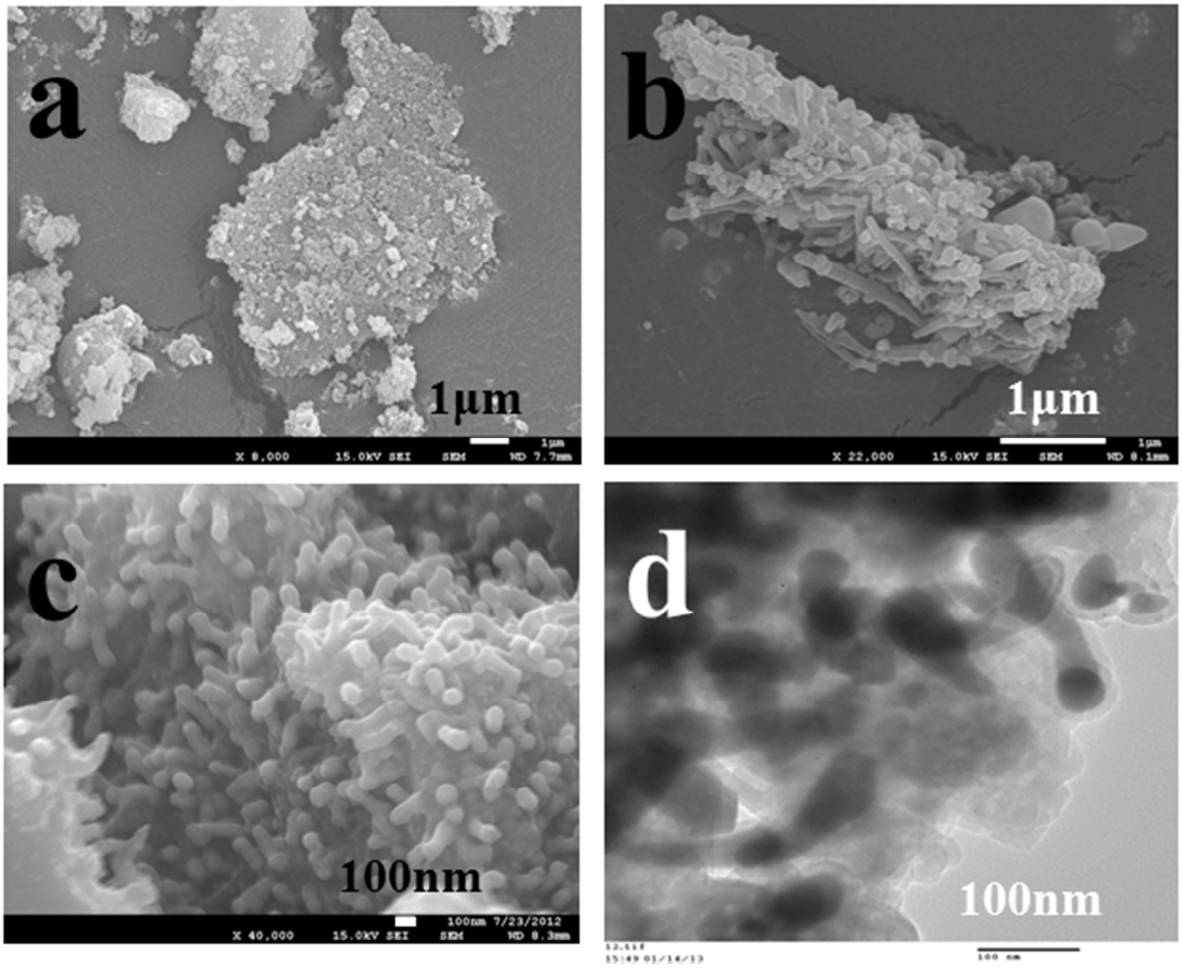

Figure 5. (a) FESEM image of SnO_2 nanoparticle decorated Si flakes, Si@SnO_2; FESEM images at (b) low magnification overall view and (c) high magnification view revealing the densely formed Si@Sn@CNRs; (d) TEM image of Si@Sn@CNRs flakes clearly showing the Sn@CNTs on the surface. .

The Si flakes were further tailored to make Si@Sn@CNR composites. Hybrid structures of silicon/carbon have been explored to improve the cycling performance of silicon anode. For example, silicon coated carbon nanofibers,[14] carbon nanotubes decorated with Si nanoparticles,[31] silicon@carbon core-shell nanowires,[32] the silicon@carbon yolk-shell structures have been reported achieving certain level of success.[33] Here, we explored to make composite based on the curved Si flakes by covering the Si flakes with Sn@CNRs. There are four reasons to introduce

Sn@CNRs: (1) carbon nanorods and carbon wrapping could dramatically improve the poor conductivity of Si flakes; (2) metallic Sn is not only highly conductive but also electrochemically active; (3) the nanorods could enhance the integration of the electrode by forming 1-D networks; (4) the voids between the 1-D nanorods can also accommodate the volume variation and alleviate the stress upon cycling. The SnO_2 nanoparticles decorated Si flakes are shown in Figure 5a. The decorated SnO_2 nanoparticles acted as catalyst for the growth of carbon nanorods through chemical vapor deposition (CVD) process, which is well documented.[34, 35] At the same time the SnO_2 nanoparticles were reduced to metallic Sn and wrapped inside the carbon nanorods, forming Sn@CNRs. The low magnification FESEM image of Si@Sn@CNRs showsthat a large number of carbon nanorods formed on the surface of Si flakes (Figure 5b). More details about the Sn@CNRs are revealed by magnified FESEM image in Figure 5c. One can see that Sn@CNRs densely covered the Si flakes. The Sn@CNRs are about 200 nm in length with diameter around ~70 nm. The detail of the Sn@CNRs is further revealed by TEM (Figure 5d). The different contrast in the nanorods are associated with the light contrast carbon nanorods encapsulating dark contrast metallic Sn nanorods.[34-36] The EDS analysis of the as-prepared Si@Sn@CNRs confirmed its chemical composition (Figure S1 in Supporting Information). The weight ratio of Si:Sn:C is 19:59:19. The sample will need to be further optimized to achieve better weight balanced between those elements and electrochemical performances.

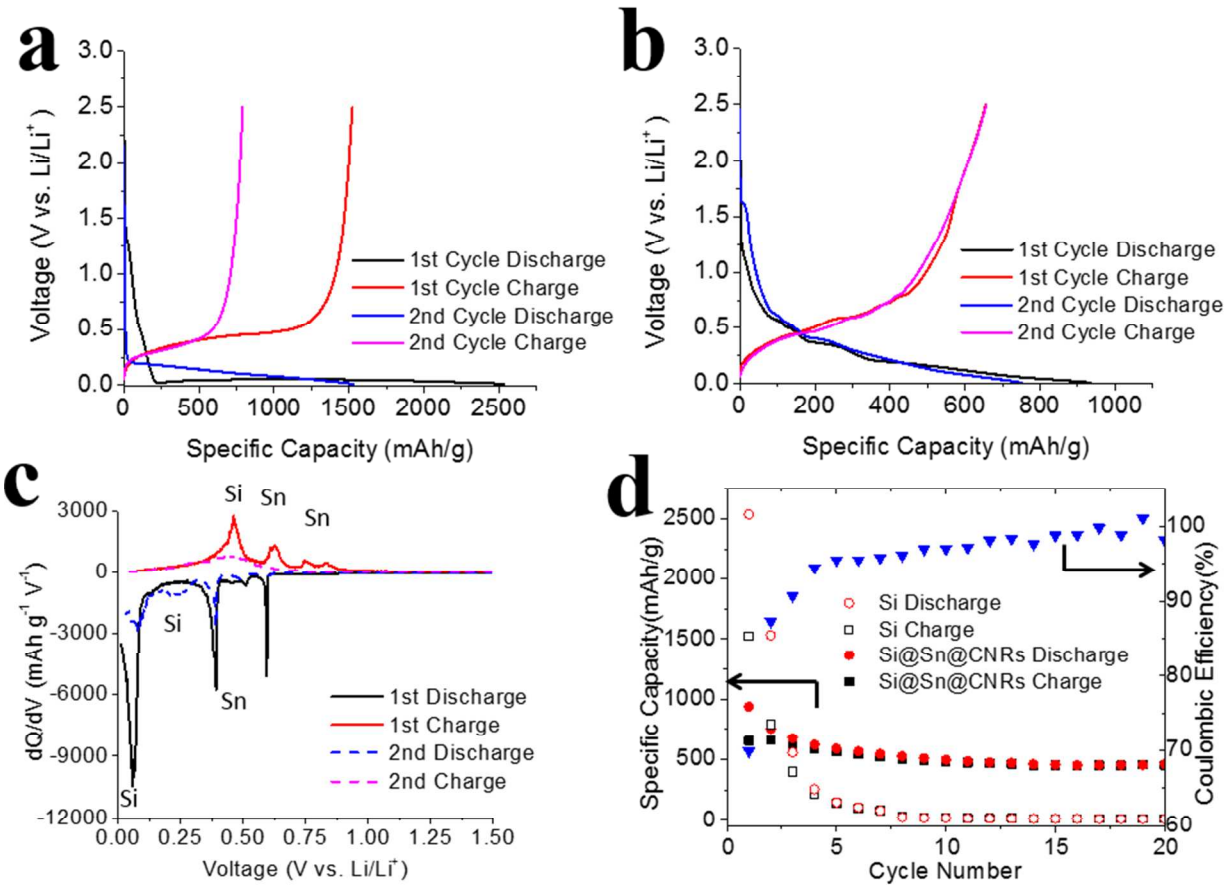

Figure 6. First two cycle charge-discharge profiles for (a) the as-prepared Si flakes and (b) the further tailored Si flakes of Si@Sn@CNRs , (c) dQ/dV for the first two cycles of Si@Sn@CNRs and (d) cyclic performance at 100 mA/g for Si flakes (hollow points) and Si@Sn@CNRs (solid points).

Electrochemical performances of the as-prepared Si flakes and the further tailored Si flakes with Sn@CNRs or Si@Sn@CNRs were thoroughly evaluated. (Figure 6) The charge-discharge profiles of both the as prepared curved Si flakes and the derived Si@Sn@CNRs were plotted in Figure 6a and Figure 6b, respectively. For Si flakes, a very long flat plateau around 0.1V is observed in the first discharge or lithiation process (black line). This plateau contributes a capacity of ~2250 mAh/g which could be attributed to the formation of Li_xSi alloy.[5, 10, 37] The

very high first cycle irreversible capacity loss of around 1000 mAh/g has been widely observed for Si anode materials, which could be attributed the formation of solid electrolyte interface (SEI) layer and the irreversible Li^+ trapping.[5, 13, 38, 39] A slope ranging from 0.25 to 0.5V was observed during the charge or de-lithiation process in the first two cycles, which could be associated with the de-alloy of Li_xSi. .[5, 10, 40]

In contrast to that of the as-prepared Si flake based anodes, no long plateau was observed in the charge-discharge profile of Si@Sn@CNRs (Figure 6b). Instead, the capacity dropped much slower to around 0.5V and a slope ranging from 0.5 to 0.01V was observed in the lithiation process for the first two cycles. The improvement of the capacity retention demonstrated that the design of unique integrated structure of Si@Sn@CNRs and the decoration of conductive 1D Sn@CNR network can effectively enhance the electrochemical performance of Si flakes. The improved performances could be attributed to the decoration of Sn@CNRs on the surface of the Si flakes where the Sn@CNRs can enhance electric conductivity, alleviate the stress, and form a network to integrate the electrodes. The initial capacity of Si@Sn@CNRs of 950 mAh/g is lower than that of pristine Si flakes, which is due to the lower theoretical capacity of both Sn and carbon as compared to the high theoretical capacity of Si of 3572 mAh/g. The theoretical specific capacity is estimated to be 1358 mAh/g based on the weight percent of C, Si, and Sn in the composite based on EDS results. Due to the aforementioned advantages offered by the metallic tin and carbon, the fast capacity fading associated with silicon is not observed. The initial capacity loss decreased from 1000 mAh/g for Si flakes to 200 mAh/g for Si@Sn@CNRs flakes, which could be attributed to the dramatically reduced SEI formation. It is known that SEI formation on the surface of carbon is different from that of Si. The formation of stable beneficial SEI layer on carbon is well documented. The SEI on carbon can facilitate the transfer of Li^+,

prevent the formation of additional SEI in subsequent cycles and enhance cyclability.[11] In contrast, the SEI layer formed on Si is relatively unstable and can be cracked due to the huge volume variation upon cycling. The SEI can continuously form upon cycling with the exposed Si to electrolytes due to racks leading to capacity fading.[33, 41, 42] Additionally, the Li^+ trapping caused by poor conductivity of Si was significantly reduced with the presence of Sn@CNR network. The charge-discharge profiles for the first two cycles almost overlapped, indicating the same electrochemical reactions involved in the first two cycles, or dramatically improved cycling performance as compared to that of pristine Si flakes. To further understand the electrochemical reactions involved for the lithium storage in Si@Sn@CNRs, the differential capacity vs. voltage plots for the first two cycles were analyzed (Figure 6c). The cathodic peaks at 0.6V and 0.38V and the anodic peaks between 0.6-0.9V can be attributed to the lithium insertion into and extraction from Sn, respectively.[43] The cathodic peaks below 0.12V and anodic peak at ~0.48V can attributed to the lithiation and de-lithiation process of silicon. [44, 45] Meanwhile, the lithium insertion into carbon composition also contribute to part of the cathodic peak below 0.12V. [46, 47]

The cycling performance of both Si flakes and Si@Sn@CNRs are compared in Figure 6d. The pure Si (hollow symbols) shows the typical cycling performance of Si material with dramatically capacity fading upon cycling. The capacity fading of Si is well documented. For example, in the case of Si microparticles, the capacity fades from ~3750 mAh/g to ~300 mAh/g;[38] And in another case of carbon-coated bulk Si, the capacity fades from 2630 mAh/g to ~300 mAh/g after 30 cycles,.[38, 39] In our case of Si flakes, it has similar large capacity for the first cycle but the irreversible capacity loss is huge. The charge capacity faded from 791 mAh/g in the 2nd cycle to 138 mAh/g after 5 cycles. As comparison, the compound of Si@Sn@CNRs has a smaller initial capacity, but the issue of fast capacity fading is significantly reduced. After 5 cycles, the specific

charge capacity of Si@Sn@CNRs just slightly faded from 654 mAh/g in the 2nd cycle to 562 mAh/g, which is much better than that of pure Si. After 20 cycles, the specific charge capacity of Si@Sn@CNRs remains at 451 mAh/g. The charge capacity retention is 69.0%. In contrast the capacity of pure Si microflakes was declined to 10 mAh/g after 20 cycles, with much smaller charge capacity retention at only 0.8%. The volumetric capacity and full-cell stack energy density were estimated to be about 647 Ah/L and 710 Wh/L.[48] The values estimated are slightly lower but still comparable to that of graphite. However, our materials have not been optimized and only 30% of the theoretical capacity was released in our preliminary study. We believe that further effort could optimize and dramatically improve their performances. The Coulombic efficiency of Si@Sn@CNRs was also shown in Figure 6d, it kept increasing for the first 10 cycles and remained at above 98% from the 10th cycle, which may due to the stabilization of SEI layer and the activation process of active materials.[49] Practically, the Coulombic efficiency obtained for our Si@Sn@CNRs sample is still not as good as required and further optimization is still needed. Addition to optimization of electrode materials, there are a few options in the preparation of the electrode and cell testing processes, including annealing PVDF binder instead of vacuum drying alone, using carboxymethyl cellulose or lithium polyacrylate as binders instead of PVDF, putting additives (such as fluoroethylene carbonate) in the conventional electrolytes, electrode activation, which are under our investigation. Here, we tried to compare the two samples tested under the same conditions. As comparison, the increasing and stabilization of Coulumbic efficiency of pure Si flakes are slower, which may due to the pulverization of Si and the continuous formation of SEI layer in the first few cycles. As compared to the pristine Si flakes, the cycling performance of Si@Sn@CNRs microflakes is significantly improved. Both samples were further tested over 60 cycles at various currents

(Figure S2 in the Supporting Information). The bare Si flakes quickly faded to insignificant capacity upon further cycling at increased currents. In contrast, the Si@Sn@CNRs microflakes could still achieve a reasonable capacity without dramatic capacity fading when the testing current was increased. The improved performances successfully verified our hypothesis discussed previously in the adoption of Sn@CNRs in to Si flakes to enhance their electrochemical performances.

4. CONCLUSION

In summary, a procedure for synthesis of curved Si flakes was developed. Commercial micro-size magnesium powder (~325 mesh) was used as bifunctional template to support the coating of SiO_2 sheath and as reductant to subsequently reduce the SiO_2 into Si via magnesiothermic reaction. Additionally, we also demonstrate a facile post-synthesis procedure to further tailor the as-prepared Si flakes by coating with Sn@CNRs making an unique composite of Si@Sn@CNRs high-order structures. Electrochemical evaluation suggests that the not-optimized Si@Sn@CNRs composite demonstrated improved Li ion storage performances. Our ongoing effort is to further investigate the effect of different Mg active template with uniquely defined structures, including various nanostructures to synthesize unique Si nanostrucutrers, and further optimize Si@Sn@CNR composites. We believe this approach could be used to synthesize Si with different nanostructures. However, the high cost will be another limitation of our approach which is worthy for further investigation and improvement.

ASSOCIATED CONTENT

Supporting Information. EDS and charge-discharge cycling test over 60 cycles under various currents.

AUTHOR INFORMATION

Corresponding Author

Da Deng, E-mail: da.deng@wayne.edu

Author Contributions

D.D. designed the research. J.Z. conducted the experiments. D.D. and J.Z. analyzed the results and wrote the manuscript.

ACKNOWLEDGMENT

The authors thank Guangzhao Mao for XRD instrument and the Lumigen Instrument Center for SEM and TEM instruments, Wayne State University, Detroit, MI.

REFERENCES

1. J. M. Tarascon and M. Armand, *Nature*, 2001, 414, 359-367.
2. M. Armand and J. M. Tarascon, *Nature*, 2008, 451, 652-657.
3. B. Dunn, H. Kamath and J.-M. Tarascon, *Science*, 2011, 334, 928-935.
4. P. G. Bruce, B. Scrosati and J.-M. Tarascon, *Angew. Chem. Int. Ed.*, 2008, 47, 2930-2946.
5. F. Cheng, J. Liang, Z. Tao and J. Chen, *Adv. Mater.*, 2011, 23, 1695-1715.
6. L. Ji, Z. Lin, M. Alcoutlabi and X. Zhang, *Energy Environ. Sci.*, 2011, 4, 2682-2699.
7. F. Liu, S. Song, D. Xue and H. Zhang, *Nanoscale Res. Lett.*, 2012, 7, 1-17.
8. A. S. Arico, P. Bruce, B. Scrosati, J.-M. Tarascon and W. van Schalkwijk, *Nat. Mater.*, 2005, 4, 366-377.
9. C. K. Chan, H. Peng, G. Liu, K. McIlwrath, X. F. Zhang, R. A. Huggins and Y. Cui, *Nat. Nanotechnol.*, 2008, 3, 31-35.
10. U. Kasavajjula, C. Wang and A. J. Appleby, *J. Power Sources*, 2007, 163, 1003-1039.
11. J. R. Szczech and S. Jin, *Energy Environ. Sci.*, 2011, 4, 56-72.
12. J. P. Maranchi, A. F. Hepp and P. N. Kumta, *Electrochem. Solid-State Lett.*, 2003, 6, A198-A201.
13. H. Jia, P. Gao, J. Yang, J. Wang, Y. Nuli and Z. Yang, *Adv. Energy Mater.*, 2011, 1, 1036-1039.
14. L.-F. Cui, Y. Yang, C.-M. Hsu and Y. Cui, *Nano Lett.*, 2009, 9, 3370-3374.
15. X. Meng and D. Deng, *ACS Appl. Mater. Interfaces*, 2015, 7, 6867-6874.
16. X. Xin, X. Zhou, F. Wang, X. Yao, X. Xu, Y. Zhu and Z. Liu, *J. Mater. Chem.*, 2012, 22, 7724-7730.

17. Z. Bao, M. R. Weatherspoon, S. Shian, Y. Cai, P. D. Graham, S. M. Allan, G. Ahmad, M. B. Dickerson, B. C. Church, Z. Kang, H. W. Abernathy Iii, C. J. Summers, M. Liu and K. H. Sandhage, *Nature*, 2007, 446, 172-175.
18. K. H. Sandhage and Z. Bao, U.S. Patent, 7615206 B2, 2009.
19. Y. Yu, L. Gu, C. Zhu, S. Tsukimoto, P. A. van Aken and J. Maier, *Adv. Mater.*, 2010, 22, 2247-2250.
20. J. Liu and X.-W. Liu, *Adv. Mater.*, 2012, 24, 4097-4111.
21. S. Liu and M. Y. Han, *Chem. Asian J.* , 2010, 5, 36-45.
22. S. Kralj, D. Makovec, S. Čampelj and M. Drofenik, *J. Magn. Magn. Mater.*, 2010, 322, 1847-1853.
23. Y. Meng, D. Chen and X. Jiao, *J. Phys. Chem. B*, 2006, 110, 15212-15217.
24. Y. Chen, X. Xue and T. Wang, *Nanotechnology*, 2005, 16, 1978.
25. Y. Ren, M. Chen, Y. Zhang and L. Wu, *Langmuir*, 2010, 26, 11391-11396.
26. K. Ding, B. Hu, Y. Xie, G. An, R. Tao, H. Zhang and Z. Liu, *J. Mater. Chem.*, 2009, 19, 3725-3731.
27. Y. Zhu, Y. Pan, H. Xu, C. Xiang, H. Kou and J. Guo, *Chem. Lett.*, 2007, 36, 1098-1099.
28. T.-D. Nguyen, J. A. Kelly, W. Y. Hamad and M. J. MacLachlan, *Adv. Funct. Mater.*, 2015, DOI: 10.1002/adfm.201404304, DOI: 10.1002/adfm.201404304.
29. W. Li, C. Li, C. Zhou, H. Ma and J. Chen, *Angew. Chem. Int. Ed.*, 2006, 45, 6009-6012.
30. B. Peng, J. Liang, Z. Tao and J. Chen, *J. Mater. Chem.*, 2009, 19, 2877-2883.
31. A. Gohier, B. Laïk, K.-H. Kim, J.-L. Maurice, J.-P. Pereira-Ramos, C. S. Cojocaru and P. T. Van, *Adv. Mater.*, 2012, 24, 2592-2597.
32. H. Kim and J. Cho, *Nano Lett.*, 2008, 8, 3688-3691.
33. N. Liu, H. Wu, M. T. McDowell, Y. Yao, C. Wang and Y. Cui, *Nano Lett.*, 2012, 12, 3315-3321.
34. D. Deng, M. G. Kim, J. Y. Lee and J. Cho, *Energy Environ. Sci.*, 2009, 2, 818-837.
35. D. Deng and J. Y. Lee, *J. Mater. Chem.*, 2010, 20, 8045-8049.
36. Y. Zou and Y. Wang, *ACS Nano*, 2011, 5, 8108-8114.
37. L.-F. Cui, L. Hu, J. W. Choi and Y. Cui, *ACS Nano*, 2010, 4, 3671-3678.
38. C. Wang, H. Wu, Z. Chen, M. T. McDowell, Y. Cui and Z. Bao, *Nat. Chem.*, 2013, 5, 1042-1048.
39. H. Yoo, J.-I. Lee, H. Kim, J.-P. Lee, J. Cho and S. Park, *Nano Lett.*, 2011, 11, 4324-4328.
40. A. Rong, X. P. Gao, G. R. Li, T. Y. Yan, H. Y. Zhu, J. Q. Qu and D. Y. Song, *J. Phys. Chem. B*, 2006, 110, 14754-14760.
41. B. Liu, P. Soares, C. Checkles, Y. Zhao and G. Yu, *Nano Lett.*, 2013, 13, 3414-3419.
42. K. Fu, O. Yildiz, H. Bhanushali, Y. Wang, K. Stano, L. Xue, X. Zhang and P. D. Bradford, *Adv. Mater.*, 2013, 25, 5109-5114.
43. W.-M. Zhang, J.-S. Hu, Y.-G. Guo, S.-F. Zheng, L.-S. Zhong, W.-G. Song and L.-J. Wan, *Adv. Mater.*, 2008, 20, 1160-1165.
44. M. K. Datta and P. N. Kumta, *J. Power Sources*, 2009, 194, 1043-1052.
45. A. M. Chockla, J. T. Harris, V. A. Akhavan, T. D. Bogart, V. C. Holmberg, C. Steinhagen, C. B. Mullins, K. J. Stevenson and B. A. Korgel, *J. Am. Chem. Soc.*, 2011, 133, 20914-20921.
46. J. Y. Eom, H. S. Kwon, J. Liu and O. Zhou, *Carbon*, 2004, 42, 2589-2596.
47. G. T. Wu, C. S. Wang, X. B. Zhang, H. S. Yang, Z. F. Qi, P. M. He and W. Z. Li, *J. Electrochem. Soc.*, 1999, 146, 1696-1701.
48. M. N. Obrovac and V. L. Chevrier, *Chemical Reviews*, 2014, 114, 11444-11502.
49. J. Hassoun, F. Bonaccorso, M. Agostini, M. Angelucci, M. G. Betti, R. Cingolani, M. Gemmi, C. Mariani, S. Panero, V. Pellegrini and B. Scrosati, *Nano Lett.*, 2014, 14, 4901-4906.